ELSEVIER

Journal of Alloys and Compounds 280 (1998) 44–55

Journal of ALLOYS AND COMPOUNDS

On the magnetic ordering of $R_6Fe_{13}X$ compounds

P. Schobinger-Papamantellos[a,*], K.H.J. Buschow[b], C.H. de Groot[b], F.R. de Boer[b], C. Ritter[c], F. Fauth[c], Grit Boettger[c]

[a]*Laboratorium für Kristallographie, ETHZ CH-8092 Zürich, Switzerland*
[b]*Van der Waals-Zeeman Institute, University of Amsterdam, Valckenierstr. 65, 1018 XE Amsterdam, The Netherlands*
[c]*Institut Laue-Langevin, 156X, 38042 Grenoble Cédex, France*

Received 25 June 1998

Abstract

Neutron diffraction performed on $Pr_6Fe_{13}Ag$ and $Pr_6Fe_{13}Au$ powder samples reveals a collinear antiferromagnetic ordering of the four Fe and the two Pr sublattices associated with the wave vector $q=(001)$ (I_P magnetic lattice with anticentering translation). The moments of all sublattices located at ($xy0$) layers, sandwiched between successive X layers perpendicular to z at $z=-0.25$, 0.25, are confined to the same direction within the ($xy0$) plane. They change their direction collectively when going to the next Ag(Au) layers at $z=0.25$, 0.75. The Pr moments at 1.5 K are $2.5(2)\mu_B$ and $2.6(1)\mu_B$/Pr atom, while the average Fe ordered value is $2.2\mu_B$/Fe atom, in agreement with Mössbauer results. Detailed results are presented for $Pr_6Fe_{13}Ag$.

Keywords: Antiferromagnetic ordering; Crystal structure; Magnetic structure; Neutron diffraction; $Pr_6Fe_{13}Ag$; $Pr_6Fe_{13}Au$

1. Introduction

Rare earth (R) compounds of the type $R_6Fe_{13}X$ (X=Cu, Ag, Au, Si, Sn...) crystallise in the tetragonal $Nd_6Fe_{13}Si$ structure [1,2] in space group *I4/mcm*. This structure is an ordered variant of the $La_6Co_{11}Ga_3$ structure [3] with two rare earth sites, R_1 (8f) and R_2 (16l), and four Fe sites, Fe_1 (4d), Fe_2 (16k), Fe_3 ($16l_1$) and Fe_4 ($16l_2$). These compounds form only for the first few members of the rare earth series, and their magnetic properties were studied earlier by Weitzer et al. [2]. According to the latter authors the $Nd_6Fe_{13}X$ compounds order magnetically below $T_C=$ 340 K, the magnetic ordering being revealed by a rise of the magnetisation below T_C. Yan et al. [4] and Fangwei Wang et al. [5] report, on the basis of neutron and X-ray data, a collinear ferrimagnetic moment arrangement for $Nd_6Fe_{13}Si$ and $Pr_6Fe_{13}Si$ with the moments forming two antiferromagnetically coupled sublattices: $R_1(8f)\uparrow$, $R_2(16l)\uparrow$, $Fe_1(4d)\uparrow$, $Fe_2(16k)\downarrow$, $Fe_3(16l_1)\downarrow$, $Fe_4(16l_2)\downarrow$, pointing along *c* as suggested in Ref. [6].

More recent measurements have indicated quite different magnetic behaviour, characterised by a Néel-type transition at much higher temperatures, typically 410 K [7]. Also, Mössbauer spectroscopy [7] confirmed that the magnetic ordering in $Nd_6Fe_{13}Au$ occurs at a much higher temperature than reported previously. Interestingly, the value of the average Fe moment of $1.9\mu_B$ found from high-field measurements and Mössbauer spectroscopy in $Nd_6Fe_{13}Au$ is much higher than in the RFe_2 compounds ($1.5\mu_B$ per Fe atom) even though the Fe concentration is about the same.

Of particular interest is the fact that the higher Fe moments in $R_6Fe_{13}X$ lead to antiferromagnetic order with T_N around 400 K as compared to ferromagnetic order ($T_C>600$ K) in RFe_2. The occurrence of antiferromagnetic interactions in Fe-based compounds is of general interest with regard to the validity of the Néel–Slater type approach to make predictions on the magnetic interactions of metallic Fe-based systems.

In the present neutron diffraction investigation we report on the magnetic ordering of two $R_6Fe_{13}X$ compounds (X=Ag, Au) in order to elucidate the controversy between the results obtained by macroscopic and microscopic methods as given above. More detailed neutron diffraction results will be given presently for the $Pr_6Fe_{13}Ag$ compound.

*Corresponding author.

0925-8388/98/$ – see front matter
PII: S0925-8388(98)00712-9

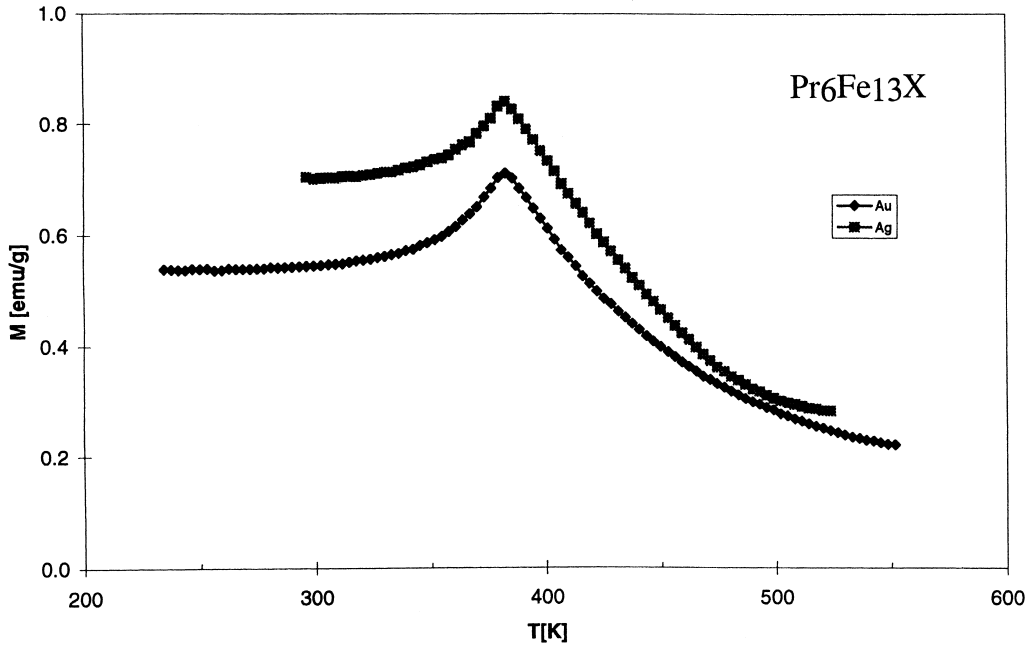

Fig. 1. Temperature dependence of the magnetisation above room temperature for the compounds $Pr_6Fe_{13}Ag$ and $Pr_6Fe_{13}Au$.

2. Sample preparation and magnetic measurements

The $Pr_6Fe_{13}Ag$ and $Pr_6Fe_{13}Au$ samples were prepared by arc melting starting materials of at least 99.9% purity. In order to suppress the formation of compounds of the 2:17-type as far as possible we used an excess of about 2% of Pr. After arc melting, the samples were wrapped in Ta foil, sealed in an evacuated quartz tube and annealed for about 3 weeks at 800°C. After annealing, the samples were quenched to room temperature by breaking the quartz tubes in water. X-ray diffraction diagrams showed that the annealed samples were approximately single phase, their crystal structure corresponding to the tetragonal $Nd_6Fe_{13}Si$ structure type. In order to determine the magnetic ordering temperature of the two compounds investigated we performed magnetic measurements above 300 K on a home-built magnetometer based on the Faraday principle, using polycrystalline lumps in order to avoid oxidation at elevated temperatures as far as possible. Results of the magnetic measurements are displayed in Fig. 1. It can be derived from these measurements that both compounds show a Néel-type magnetic ordering transition at $T_N = 380$ K.

3. Neutron diffraction

Neutron diffraction experiments were carried out on powder samples of $Pr_6Fe_{13}Ag$ and $Pr_6Fe_{13}Au$ in the temperature range 1.5–450 K. The data were collected with the D1A and D1B (double axis multicounter diffractometers) at the facilities of the ILL in Grenoble using a wavelength of 1.9114 and 2.531 Å, respectively. The step increment of the diffraction angle 2θ was 0.05° and 0.1° for the D1A data and 0.2° for the D1B data. The data were corrected for absorption and evaluated by the FullProf Program [8]. The high resolution (HR) data obtained in the 0–160° 2θ range with the D1A instrument were used for structural (nuclear and magnetic) refinements for a few temperatures. The D1B data were collected with a 5–10 K step in temperature (2θ range 2–82°) in order to derive the magnetic phase diagram. In the 110 K data taken on the D1B instrument, due to the high neutron flux, one observes an overlapping vanadium peak at 72° from the V sample holder.

3.1. Nuclear structure of $Pr_6Fe_{13}Ag$ (HR 420 K data $\lambda = 1.9114$ Å)

The neutron diffraction pattern recorded in the paramagnetic state at 420 K is shown in the top part of Fig. 2. The refined parameters given in Table 1 confirm the structure type [1,2]. The *R*-factor values are satisfactory and indicate no other significant deviation from the basic structure. Some overlapping impurity lines are visible in the difference diagram around 55°.

3.2. Magnetic ordering of $Pr_6Fe_{13}Ag$ ($\mathbf{q}=0,0,1$) HR data $\lambda = 1.9114$ Å)

As can be seen from Figs. 2 and 3, the main feature of all the patterns collected at various temperatures in the magnetically ordered state is the presence of a dominant (001) reflection at $2\theta = 4.8°$, while the other magnetic contributions are difficult to discern from the nuclear reflections at higher angles. This suggests low magnetic

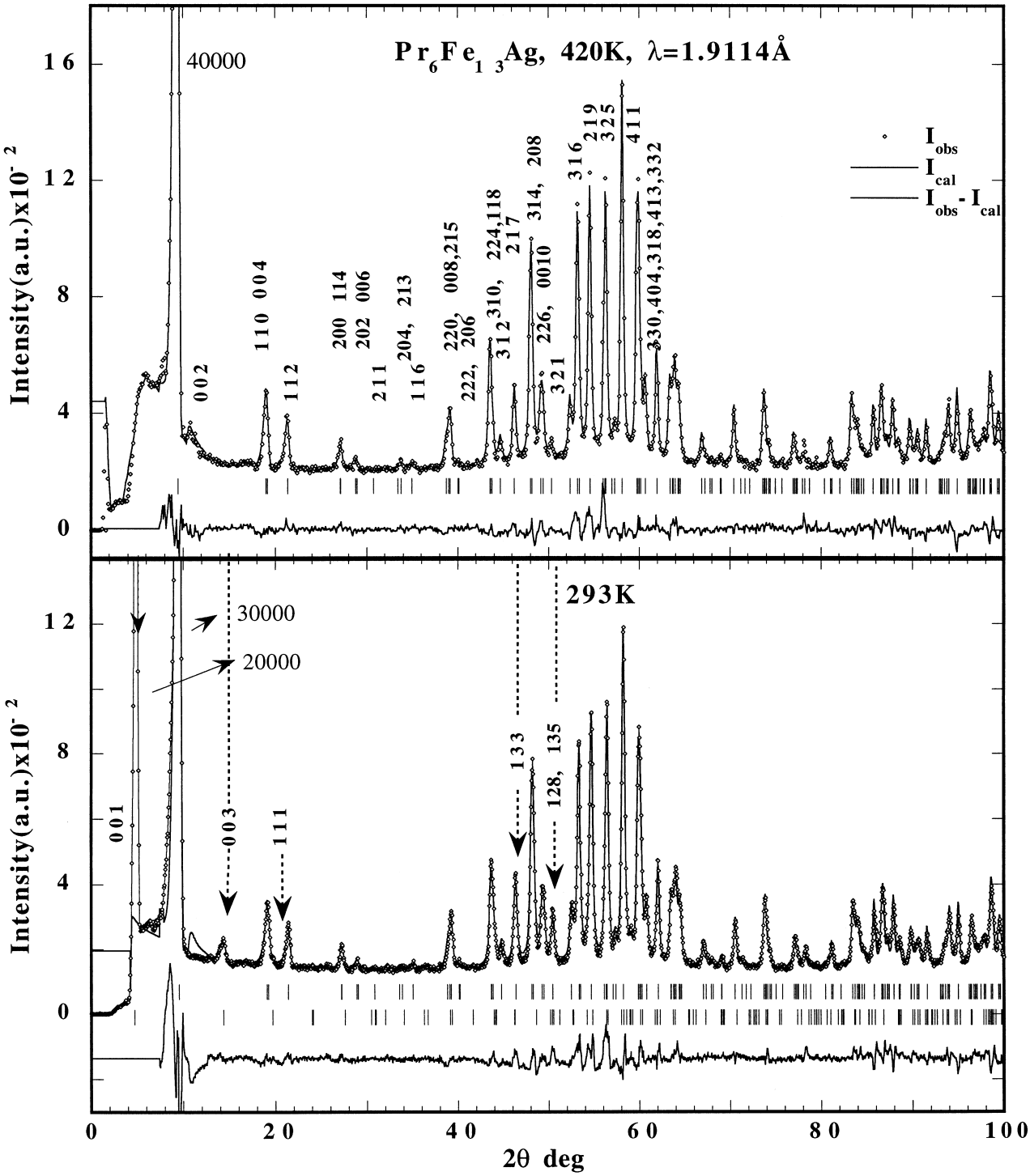

Fig. 2. Part of the observed, calculated and difference neutron HR patterns (D1A diffractometer) for $Pr_6Fe_{13}Ag$ in the paramagnetic state at 420 K and the magnetically ordered state at 293 K. The strongest magnetic reflections are indicated by arrows.

intensity values which are encumbering the data analysis as the weak magnetic reflections may overlap with the stronger nuclear reflections in view of the large lattice constants. Without the (001) reflection, the percentage of magnetic intensities does not exceed 6%, while including the (001) reflection it becomes over 40%. On the other hand, the peak shape of this reflection (excluded from the refinements) is far from Gaussian due to defects of the neutron optic system of the D1A instrument and most likely a part of this reflection is reduced by the beam cutter. For similar reasons, the strong asymmetry of the first nuclear reflection cannot be fitted properly. The inclusion of the first peak in the refinements was effected only for the D1B data, shown in the top part of Fig. 4. The

Table 1
Refined structural parameters for $Pr_6Fe_{13}Ag$ (*I4/mcm*) from HR neutron data in the paramagnetic state at 420 K and the magnetically ordered state at 293, 1.5, 40 and 120 K. μ_{xy} is the refined moment component within the tetragonal plane. Also included is a refinement based on D1B (high flux, data 110 K)

Atom/site	*x*	*y*	*z*	*B* (nm^2) ($\times 10^2$)	*x*	*y*	*z*	μ_{xy} (μ_B)	*B* (nm^2) ($\times 10^2$)	*x*	*y*	*z*	μ_{xy} (μ_B)	*B* (nm^2) ($\times 10^2$)
420 K (HR, D1A)					*293 K (HR, D1A)*					*120 K (HR, D1A)*				
Pr1 8f	0	0	0.1082(5)	2.7(1)	0	0	0.1091(5)	1.5(2)	2.0(2)	0	0	0.1097(6)	2.5(2)	1.2(1)
Pr2 16l	0.1610(6)	0.6610(6)	0.1872(3)	2.7(1)	0.1621(7)	0.6621(7)	0.1883(3)	0.4(2)	2.0(2)	0.1631(8)	0.6625(8)	0.1886(4)	1.8(1)	1.2(1)
Fe1 4d	0.0	0.5	0.0	1.8(1)	0	0.5	0	1.1(2)	1.6(1)	0	0.5	0	1.0(2)	1.0(1)
Fe2 16k	0.0685(4)	0.2087(4)	0.0	1.8(1)	0.0678(5)	0.2091(5)	0	2.1(2)	1.6(1)	0.0677(6)	0.2092(6)	0	2.0(2)	1.0(1)
Fe3 16l$_1$	0.1770(3)	0.1770(3)	0.0596(1)	1.8(1)	0.1772(3)	0.6772(3)	0.0610(3)	2.9(2)	1.6(1)	0.1775(4)	0.6775(4)	0.0606(2)	2.1(1)	1.0(1)
Fe4 16l$_2$	0.3830(3)	0.8830(3)	0.0956(1)	1.8(1)	0.3847(3)	0.8847(3)	0.0975(3)	3.2(2)	1.6(1)	0.3850(4)	0.8850(4)	0.0971(2)	2.1(2)	1.0(1)
Ag 4a	0.0	0.0	0.25		0	0	0.25		1.6(3)	0	0	0.25		0.9(3)
a, *c* (nm)	0.81181(2)	2.2810(1)			0.81188(2)	2.2816(1)				0.81119(4)	2.2723(1)			
R_n, R_m, R_{wp}, R_{exp} (%)	6, –, 9 2				5.9, 10, 19, 6					5, 12, 15, 5				
40 K (HR, D1A)				μ_{xy} (μ_B)	*1.5 K (HR, D1A)*					*110 K (D1B)*				
Pr1 8f	0	0	0.1090(2)	2.8(1)	0	0	0.1099(9)	2.6(2)	1.2(2)	0	0	0.1100	3.3(2)	0.17
Pr2 16l	0.1636(9)	0.6636(9)	0.1882(4)	2.1(1)	0.1637(8)	0.6637(8)	0.1883(4)	2.5(1)	1.2(2)	0.1630	0.6631	0.1886	1.9(1)	0.17
Fe1 4d	0	0.5	0	1.4(1)	0	0.5	0	0.9(2)	1.2(1)	0	0.5	0	1.3(2)	0.17
Fe2 16k	0.0679(7)	0.2104(7)	0	1.6(2)	0.0675(7)	0.2095(6)	0	2.1(2)	1.2(1)	0.0678	0.2087	0	1.1(1)	0.17
Fe3 16l$_1$	0.1774(5)	0.6775(5)	0.0611(3)	2.0(2)	0.1770(5)	0.6770(5)	0.0608(2)	2.3(1)	1.2(1)	0.1770	0.6772	0.0611	2.3(1)	0.17
Fe4 16l$_2$	0.3847(5)	0.8847(5)	0.0975(2)	2.2(1)	0.3844(5)	0.8844(5)	0.0976(2)	2.3(1)	1.2(1)	0.3847	0.8847	0.0975	2.2(1)	0.17
Ag 4a		0	0.25		0	0	0.25		1.2(4)	0	0	0.25		0.17
a, *c* (nm)	0.81102(5)	2.2687(2)			0.81104(5)	2.2685(2)				0.81045(6)	2.2671(2)			
R_n, R_m, R_{wp}, R_{exp} (%)	6, 14, 18, 7				6, 12, 14, 5					4.3, 1.6, 5.8, 1				

results are included in Table 3 for comparison with the D1A results obtained in the same temperature range.

The presence of odd (00*l*) reflections suggests a purely antiferromagnetic structure with the wave vector $q=(0,0,1)$. The *I* centering condition ($h+k+l=2n$) is not fulfilled and the magnetic lattice denoted by I_P [9,10] has a (1/2,1/2,1/2) antitranslation. Furthermore, the strong observed (001) intensity suggests that the main axis of antiferromagnetism is confined to the (001) plane.

Symmetry analysis suggests 10 possible magnetic space groups, eight corresponding to one-dimensional and two corresponding to two-dimensional representations. The former are identical to the Shubnikov groups [9,10] which are listed in Table 2 with the corresponding magnetic modes. Because Pr1 at (8f) is situated on the tetragonal (00*z*) axis the groups 5–8 can be ruled out as they comprise a 4′ axis which does not leave the moment of the Pr1 at 8(a) invariant. On the other hand, none of the other groups allows a mode along *x* or *y* that may give rise to the (001) reflection. This means that there is a further symmetry lowering to one of the orthorhombic subgroups of order two not comprising the four-fold axis such as *I2/m2/c21* (*Ibam*) or *I2/m12/m* (*Fmmm*).

In order to derive in a first approximation a model for the magnetic ordering we chose a more pragmatic way based on the observed intensities of a set of six (00*l*) reflections and compared these with the calculated structure factors, which depend exclusively on the atomic *z* parameters. As can be seen from Table 2, due to the layered nature of the structure along *z* the data analysis is simplified by the fact that there are only four atomic layers at (1) *z* and (2) $1/2-z$; and their centrosymmetric counterparts at (3) $-z$ and (4) $z-1/2$. The *I* antitranslation moves atoms of layer (1)→(4) and atoms of layer (2)→(3). The magnetic structure factor of the (00*l*) reflections of any Wyckoff site will be proportional to the expression:

$$2nf_j(\boldsymbol{m}_1 e^{-2\pi ilz} + \boldsymbol{m}_2 e^{-2\pi il(1/2-z)} + \boldsymbol{m}_3 e^{2\pi ilz} + \boldsymbol{m}_4 e^{2\pi il(1/2-z)}) \quad (1)$$

where 2 indicates the anticentering translation and *n* 1/8 of the site multiplicity. $\boldsymbol{m}_i$ is the magnetic moment vector of a site and f_j the magnetic form factor.

For $l=$ odd expression (1) equals:

$$2n(\boldsymbol{m}_1 e^{-2\pi ilz} - \boldsymbol{m}_2 e^{2\pi ilz} + \boldsymbol{m}_3 e^{2\pi ilz} - \boldsymbol{m}_4 e^{-2\pi ilz}) \quad (2)$$

$$2n(m_1 - m_2 + m_3 - m_4)\cos 2\pi ilz = 8nm_i \cos 2\pi ilz \text{ for a } (+\ -\ +\ -) \text{ mode along } x \quad (3)$$

$$2n(-m_1 - m_2 + m_3 + m_4)i \sin 2\pi ilz = 8nm_i \sin 2\pi ilz \text{ for a } (+\ +\ -\ -) \text{ mode along } y \quad (4)$$

This shows that the (00*l*) reflections may have intensity contributions when the intralayer coupling of the moments of a given site is ferromagnetic and the interlayer moment coupling for layers 1–4 follows the sequence (+ − + −)

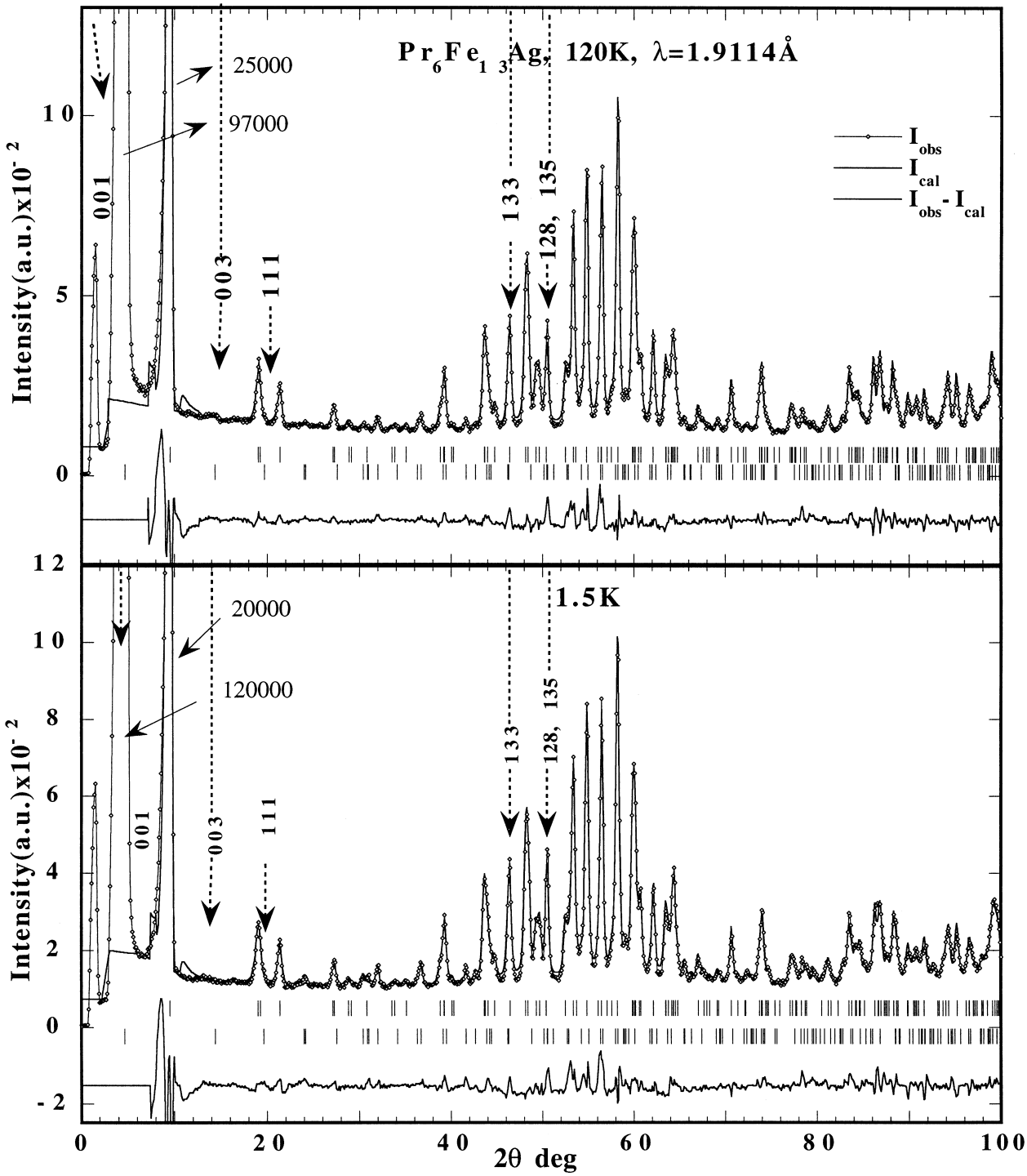

Fig. 3. Part of the observed, calculated and difference neutron HR patterns (D1A diffractometer) for $Pr_6Fe_{13}Ag$ in the magnetically ordered state at 120 and 1.5 K. The strongest magnetic reflections are indicated by arrows.

for the real part and $(+++-)$ for the imaginary part of the structure factor. The refinement has shown that the $(+-+-)$ mode is in better agreement with the observations. Table 3 shows that the strong intensity of the (001) and the weak intensity of the (003) reflections are more compatible with the cosine term.

3.2.1. The magnetic structure of $Pr_6Fe_{13}Ag$

As already mentioned, the anticentering translation *I* moves an atom of layer (1) to layer (4) and an atom of layer (2) to layer (3) and its moment changes sign. This means that when the interlayer coupling follows the $(+-+-)$ mode (giving rise to only the cosine term in the

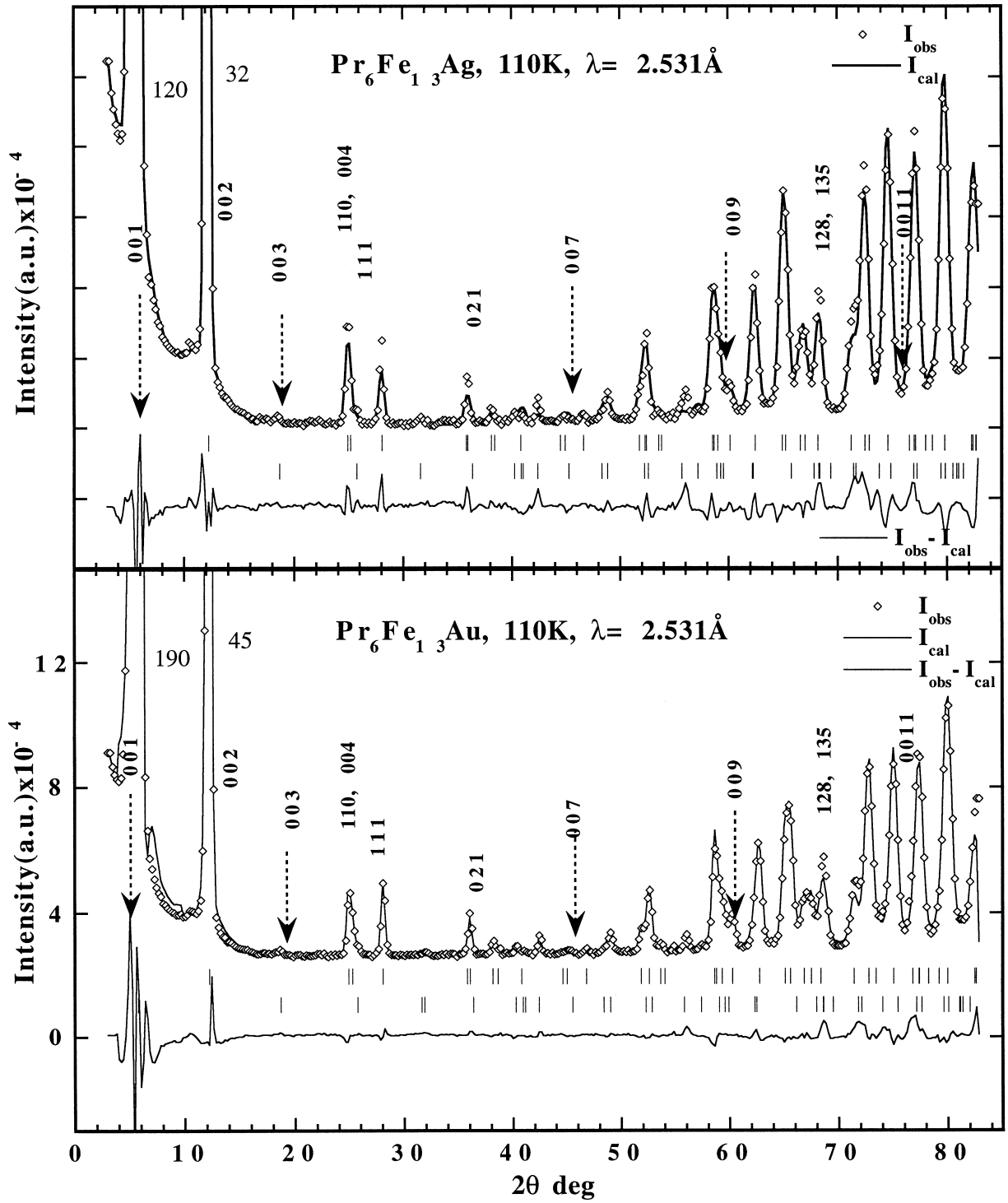

Fig. 4. Observed, calculated and difference neutron high flux patterns (D1B diffractometer) for $Pr_6Fe_{13}Ag$ and $Pr_6Fe_{13}Au$ in the magnetically ordered state at 110 K. The (00*l*) magnetic reflections are indicated by arrows.

structure factor) the intralayer coupling is ferromagnetic. Thus the moments of each site are arranged in four successive ferromagnetic layers coupled antiferromagnetically along c in the sequence $(+--+)$. The sign sequence refers to the layers at (1) z, (2) $1/2-z$, (4) $1/2+z$; (3) $-z$. Furthermore, the refinement has shown that the moments of the six sublattices (two for Pr and four for Fe) have their moments parallel within the (001) plane while the absolute direction relative to the a or b axes cannot be defined from powder diffraction. If the moments are parallel to the a or b axes the magnetic space group is $I_Pba'm'$ or $I_Pb'am'$ (Sh_{60}^{432}), respectively. For a general

Table 2
Colums 5–9: the possible magnetic space groups and corresponding magnetic modes (without the $I=1/2\ 1/2\ 1/2$ antitranslation) for the general position 32(m) of the *I4/mcm* space group associated with the wave vector $q=(001)$ I_P lattice. Column 4 describes the observed u,v modes of the realised collinear magnetic structure in the plane (001)

No.	Gen el.	*I4/mcm*			Collinear model	$I_P4/mcmi$ (Sh_{124}^{362})				$I_P4/m'c'm'i'$ (Sh_{125}^{374})				$I_P4/mc'm'i$ (Sh_{127}^{398})				$I_P4/m'cmi'$ (Sh_{130}^{434})				$I_P4'/m'c'mi$ (Sh_{133}^{470})				$I_P4'/m'cm'i'$ (Sh_{138}^{530})				$I_P4'/mcm'i$ (Sh_{132}^{458})				$I_P4'/mc'mi'$ (Sh_{135}^{494})			
1	e	x	y	z	+u	+v	+u	+v	+w	+u	+v	+w	+u	+v	+w	+u	+v	+w	+u	+v	+w	+u	+v	+w	+u	+v	+w	+u	+v	+w	+u	+v	+w	+u	+v	+w
2	2_z	$-x$	$-y$	z	+u	+v	−u	−v	+w	−u	−v	+w	−u	−v	+w	−u	−v	+w	−u	−v	+w	−u	−v	+w	−u	−v	+w	−u	−v	+w	−u	−v	+w	−u	−v	+w
3	4^+	$-y$	x	z	+u	+v	+v	−u	+w	+v	−u	+w	−v	+u	−w	−v	+u	−w	−v	+u	−w	−v	+u	−w	−v	+u	−w	+v	−u	+w	+v	−u	+w	+v	−u	+w
4	4^-	y	$-x$	z	+u	+v	−v	+u	+w	−v	+u	+w	+v	−u	−w	+v	−u	−w	+v	−u	−w	+v	−u	−w	+v	−u	−w	−v	+u	+w	−v	+u	+w	−v	+u	+w
5	2_y	$-x$	y	$1/2-z$	− u	−v	−u	+v	−w	−u	+v	−w	−u	+v	−w	−u	+v	−w	+u	−v	+w	+u	−v	+w	+u	−v	+w	+u	−v	+w	+u	−v	+w	+u	−v	+w
6	2_x	x	$-y$	$1/2-z$	− u	−v	+u	−v	−w	+u	−v	−w	−u	−v	−w	+u	−v	−w	−u	+v	+w	−u	+v	+w	−u	+v	+w	−u	+v	+w	−u	+v	+w	−u	+v	+w
7	2_{xx}	y	x	$1/2-z$	− u	−v	+v	+u	−w	+v	+u	−w	−v	−u	+w	−v	−u	+w	+v	+u	−w	+v	−w	+u	−v	−u	+w	−v	−u	+w	−v	−u	+w	−v	−u	+w
8	2_{x-x}	$-y$	$-x$	$1/2-z$	− u	−v	−v	−u	−w	−v	−u	−w	+v	+u	+w	+v	+u	+w	−v	−u	−w	−v	−u	−w	+v	+u	+w	+v	+u	+w	+v	+u	+w	+v	+u	+w
9	i	$-x$	$-y$	$-z$	+u	+v	+u	+v	+w	−u	−v	−w	+u	+v	+w	−u	−v	−w	+u	+v	+w	−u	−v	−w	+u	+v	+w	−u	−v	−w	+u	+v	+w	−u	−v	−w
10	m_z	x	y	$-z$	+u	+v	−u	−v	+w	+u	+v	−w	−u	−v	+w	+u	+v	−w	−u	−v	+w	+u	+v	−w	−u	−v	+w	+u	+v	−w	−u	−v	+w	+u	+v	−w
11	$\bar{4}^+$	y	$-x$	$-z$	+u	+v	+v	−u	+w	−v	+u	−w	−v	+u	−w	+v	−u	+w	−v	+u	−w	+v	−u	+w	+v	−u	+w	+v	−u	+w	−v	+u	−w	+v	−u	+w
12	$\bar{4}^-$	$-y$	x	$-z$	+u	+v	−v	+u	+w	+v	−u	−w	+v	−u	−w	−v	+u	+w	+v	−u	−w	−v	+u	+w	−v	+u	+w	−v	+u	+w	+v	−u	−w	−v	+u	−w
13	c_y	x	$-y$	$z-1/2$	−u	−v	−u	+v	−w	+u	−v	+w	−u	+v	−w	−u	−v	+w	+u	−v	+w	−u	+v	−w	+u	−v	+w	−u	+v	−w	+u	−v	+w	−u	+v	−w
14	c_x	$-x$	y	$z-1/2$	−u	−v	+u	−v	−w	−u	+v	+w	+u	−v	−w	−u	+v	+w	−u	+v	+w	+u	−v	−w	−u	+v	+w	+u	−v	−w	−u	+v	+w	+u	−v	−w
15	c_{x-x}	$-y$	$-x$	$z-1/2$	−u	−v	+v	+u	−w	−v	−u	+w	−v	−u	+w	+v	+u	−w	+v	+u	−w	−v	−u	+w	−v	−u	+w	+v	+u	−w	−v	−u	+w	+v	+u	−w
16	c_{xx}	y	x	$z-1/2$	−u	−v	−v	−u	−w	+v	+u	+w	+v	+u	+w	−v	−u	−w	−v	−u	−w	+v	+u	+w	+v	+u	+w	−v	−u	−w	−v	−u	−w	−v	−u	−w

Table 3
Calculated real (cos) and imaginary (sin) parts structure factor of the (00l) axial reflections for all magnetic atoms situated at layers (1) z, (2) $1/2-z$ in $Pr_6Fe_{13}Ag$. The signs of the cos and sin terms for layers (3) $-z$ and (4) $z-1/2$ obtained by inversion of (1) and (2) are $(+-)$ and $(--)$, respectively. Also given are the observed and calculated intensities obtained from the refinement of the 1.5 K HR neutron data

Atom	z	001		003		005		007		009		0011	
		cos	sin	cos	sin	cos	sin	cos	sin	cos	sin	cos	sin
Pr11	0.11	+0.771	+0.637	−0.482	+0.876	−0.951	−0.309	+0.125	−0.992	+0.998	−0.063	+0.249	+0.969
Pr12	0.39	−0.771	+0.637	+0.482	+0.876	+0.951	−0.309	−0.125	−0.992	+0.998	−0.063	−0.249	+0.969
Pr21	0.1886	+0.376	+0.927	−0.916	−0.402	+0.937	−0.351	−0.427	+0.904	−0.325	−0.946	+0.892	+0.452
Pr22	0.3114	−0.376	+0.927	+0.916	−0.402	−0.937	−0.351	+0.427	+0.904	−0.325	−0.946	−0.892	+0.452
Fe11	0.0000	+1.0	0	+1.0	0	+1.0	0	+1.0	0	+1.0	0	+1.0	0
Fe12	0.5000	−1.0	0	−1.0	0	−1.0	0	−1.0	0	−1.0	0	−1.0	0
Fe21	0.0000	+1.0	0	+1.0	0	+1.0	0	+1.0	0	+1.0	0	+1.0	0
Fe22	0.5000	−1.0	0	−1.0	0	−1.0	0	−1.0	0	−1.0	0	−1.0	0
Fe31	0.0610	+0.927	+0.374	+0.409	+0.913	−0.339	+0.941	−0.897	+0.443	−0.953	−0.303	−0.476	−0.879
Fe32	0.4390	−0.927	+0.374	−0.409	+0.913	+0.339	+0.941	+0.897	+0.443	+0.953	−0.303	+0.476	−0.879
Fe41	0.0975	+0.818	+0.575	−0.264	+0.965	−0.997	+0.078	−0.412	−0.911	+0.718	−0.696	+0.898	+0.440
Fe42	0.4025	−0.818	+0.575	+0.264	+0.965	+0.997	+0.078	+0.412	−0.911	−0.718	−0.696	−0.898	+0.440
I_{obs}, 1.5 K, 2θ (deg)		831.3	4.83	0.98	14.55	0.06	24.36	1.0	34.3	0.4	44.6	1.6	55.32
I_{calc}		830.0		0.64		0		0.6		0.4		1.7	

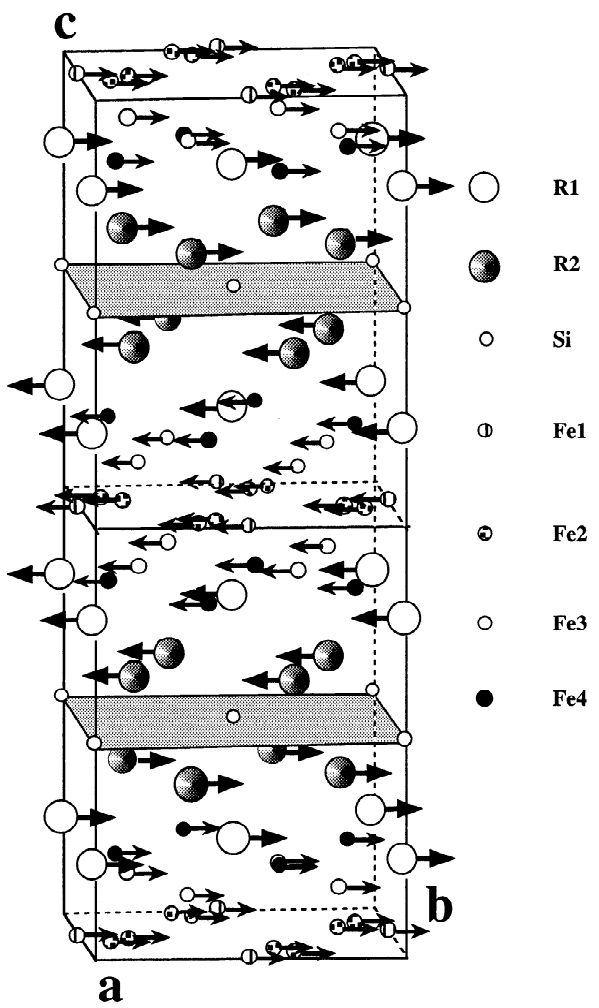

Fig. 5. Schematic representation of the collinear antiferromagnetic structures of $Pr_6Fe_{13}Ag$ and $Pr_6Fe_{13}Ag$ with the moments confined to the (001) plane.

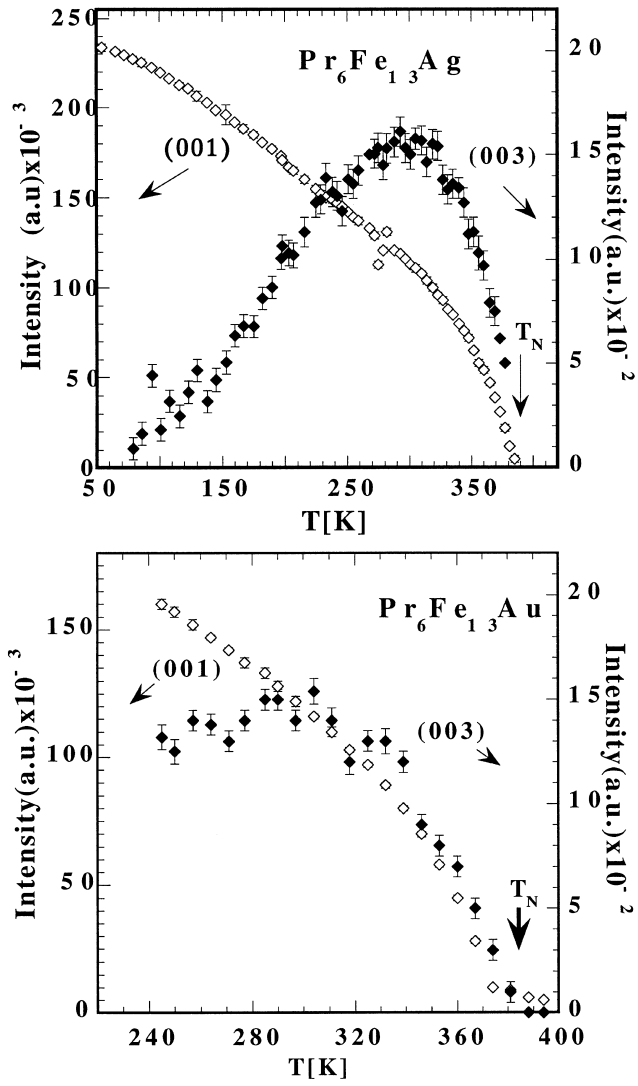

Fig. 6. Temperature dependence of the integrated intensities of several (00l) magnetic reflections of $Pr_6Fe_{13}Ag$ and $Pr_6Fe_{13}Au$.

direction in the (*xy*0) plane a further symmetry reduction has to be considered.

A simple description of the magnetic structure can be given by considering that the parallel moments within the mentioned six sublattices form ferromagnetic blocks. Each of these ferromagnetic blocks is embedded between two successive X layers perpendicular to *z* located at $z = -$ 0.25, 0.25, 0.75. The moments in these blocks change their sign collectively when going to the next block along *c*. This structure is shown in Fig. 5.

The refined parameters for various temperatures are summarised in Table 1. From the relative moment values one realises that the moments at the Pr2 site are most affected, being almost zero at 293 K. The Fe1 moment has

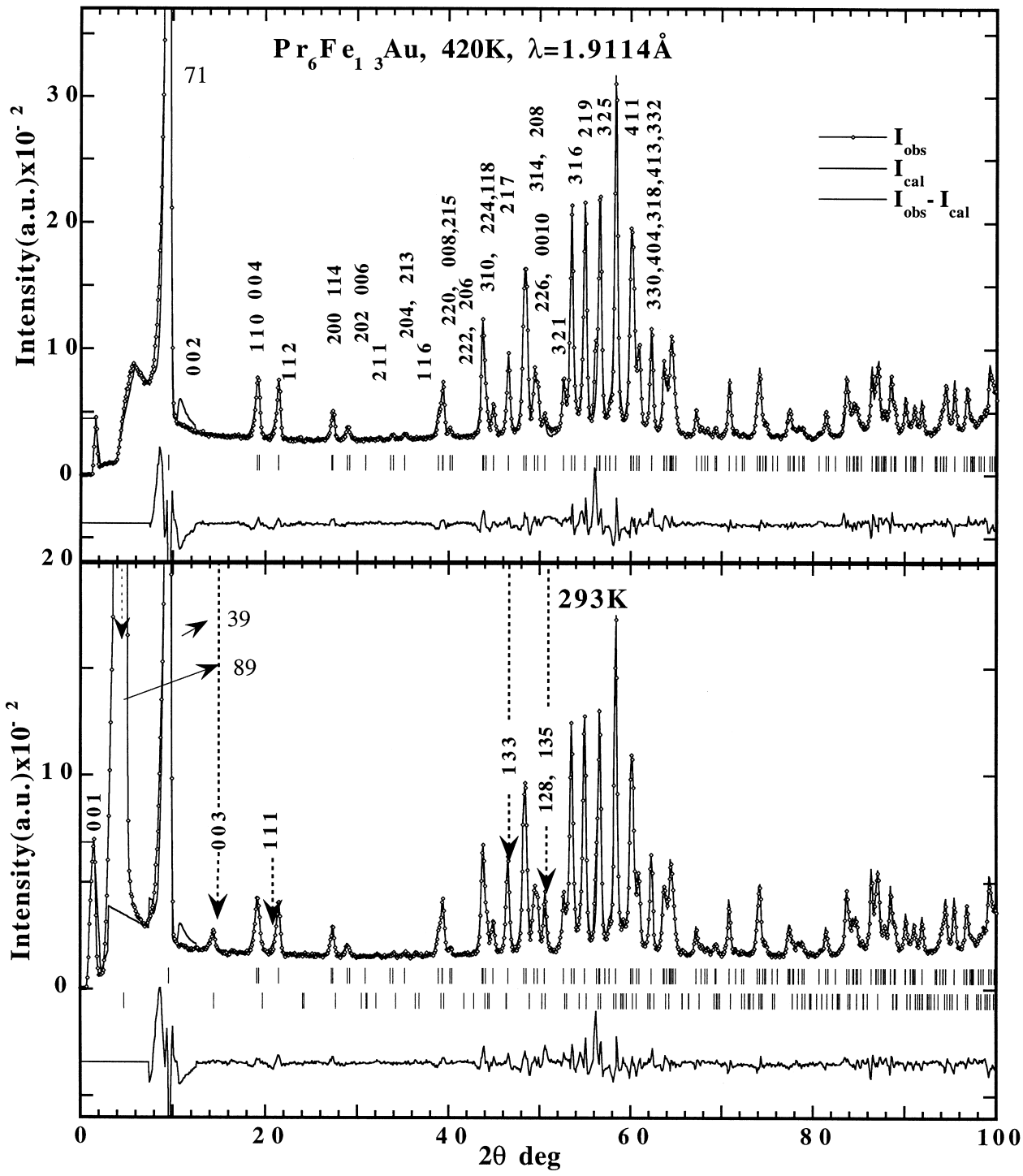

Fig. 7. Part of the observed, calculated and difference neutron HR patterns (D1A diffractometer) for $Pr_6Fe_{13}Au$ in the paramagnetic state at 410 K and the magnetically ordered state at 293 K. The strongest magnetic reflections are indicated by arrows.

the lowest average value while the other three Fe sites have already at 120 K reached the saturation value of $2.3(1)\mu_B$ within experimental error. At 1.5 K, the moments of both Pr sites ($2.6(1)\mu_B$) are still below the free ion value, $gJ\mu_B = 3.2\mu_B$, which is most probably due to crystal field effects. However, when comparing the D1B refined data at 110 K and the 120 K D1A data one obtains a slightly higher average moment value for Pr1 and a slightly lower Fe2 moment value.

3.2.2. Temperature evolution of magnetic order in $Pr_6Fe_{13}Ag$

The thermal behaviour of the (001) and (003) magnetic reflections displayed in the top part of Fig. 6 is similar for all compounds. For the compound $Pr_6Fe_{13}Ag$, magnetic order occurs at 385 ± 5, as can be seen from the increase of the intensities of both reflections with decreasing temperature in the range 400–300 K. However, below about 300 K the intensity of the (003) reflection starts to decrease and almost vanishes below 100 K. This behaviour can be explained by a close inspection of the structure factor for the (003) reflection, which is given by

$$-8f_{Pr}(0.482m_{Pr1} + 2 \times 0.916m_{Pr2}) + 4f_{Fe}(m_{Fe1} + 4m_{Fe2} + 4 \times 0.409m_{Fe3} - 4 \times 0.264m_{Fe4}) \quad (5)$$

The contributions of Pr and the contributions of the three Fe sublattices have opposite signs. As the contribution of Pr2 is four times larger than that of Pr1 it is plausible to a assume that the decreasing intensity of the (003) reflection with decreasing temperature below 300 K is due to gradual ordering of the Pr2 moments. This is in good agreement with the almost zero refined moment value for this atom at 293 K.

3.3. The magnetic structure of $Pr_6Fe_{13}Au$

For the determination of the magnetic structure of $Pr_6Fe_{13}Au$ we used basically the same procedures as described above for $Pr_6Fe_{13}Ag$. Results obtained on the D1A instrument at a few relevant temperatures are displayed in Figs. 7 and 8. By comparing with the results shown for $Pr_6Fe_{13}Ag$ in Figs. 2 and 3 one notices that the diffraction data for these two compounds are virtually the same. This is also the case for the results obtained on the D1B instrument which can be compared in Fig. 4. The refined structural parameters of $Pr_6Fe_{13}Au$ are listed in Table 4. In view of the close similarity between the results obtained for both compounds we studied the temperature dependence of magnetic ordering in $Pr_6Fe_{13}Au$ only for the temperature range around the Néel temperature. These

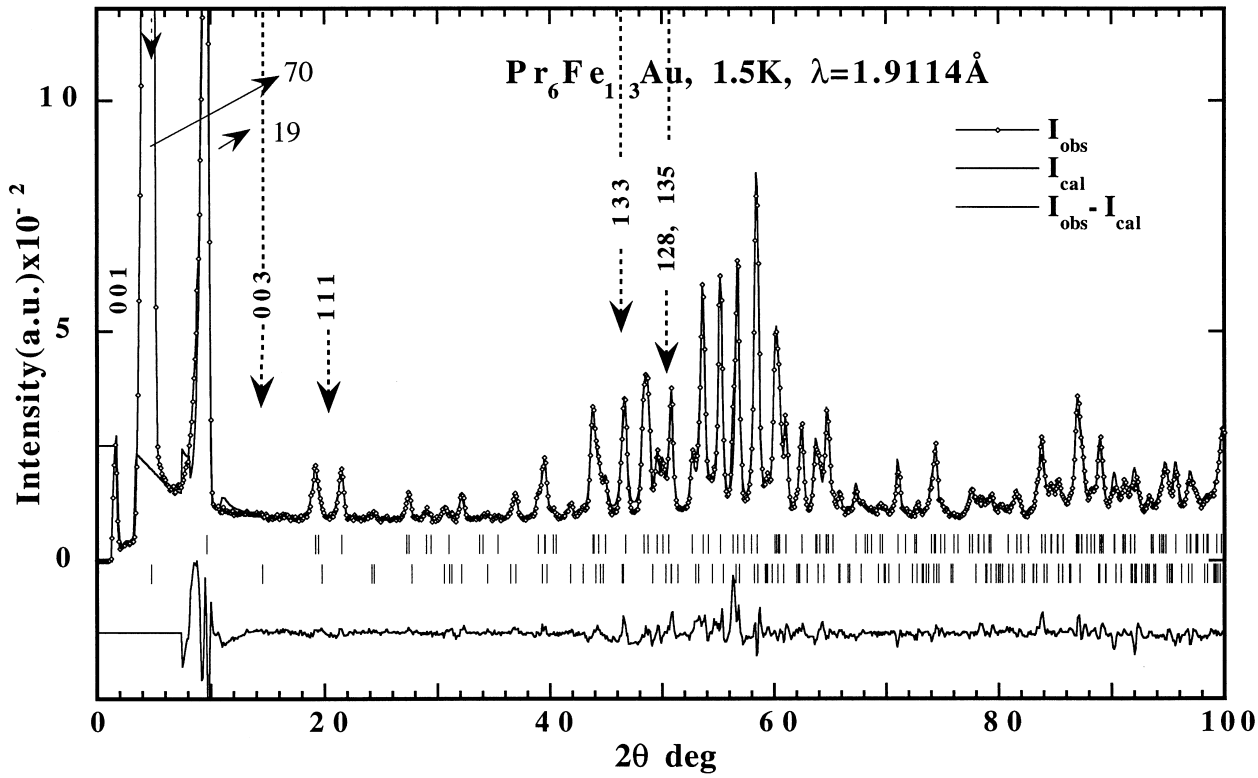

Fig. 8. Part of the observed, calculated and difference neutron HR pattern (D1A diffractometer) for $Pr_6Fe_{13}Au$ in the magnetically ordered state at 1.5 K. The strongest magnetic reflections are indicated by arrows.

Table 4
Refined structural parameters for $Pr_6Fe_{13}Au$ (*I4/mcm*) from HR neutron data in the paramagnetic state at 420 K and the magnetically ordered state at 293 and 1.5 K. μ_{xy} is the refined moment component within the tetragonal plane. Also included is a refinement based on D1B (high flux, data 110 K)

Atom/site	*x*	*y*	*z*	*B* (nm^2) ($\times 10^2$)	*x*	*y*	*z*	μ_{xy} (μ_B)	*B* (nm^2) ($\times 10^2$)
420 K (HR, D1A)					*293 K (HR, D1A)*				
Pr1 8f	0	0	0.1106(7)	2.2(1)	0	0	0.1107(6)	1.7(2)	1.5(2)
Pr2 16l	0.1631(8)	0.6631(8)	0.1894(4)	2.2(1)	0.1620(8)	0.6620(8)	0.1904(4)	0.6(2)	0.5(2)
Fe1 4d	0.0	0.5	0.0	1.4(1)	0	0.5	0	1.1(2)	0.8(2)
Fe2 16k	0.0668(6)	0.2085(5)	0	1.4(1)	0.0673(5)	0.2086(5)	0	1.5(2)	0.8(1)
Fe3 $16l_1$	0.1774(4)	0.6774(3)	0.0604(2)	1.4(1)	0.1778(4)	0.6778(4)	0.0607(2)	1.7(2)	0.8(1)
Fe4 $16l_2$	0.3845(4)	0.8845(4)	0.0962(2)	1.4(1)	0.3849(4)	0.8849(4)	0.0970(2)	1.4(2)	0.8(1)
Au 4a	0.0	0.0	0.25	1.8(3)	0	0	0.25		1.1(2)
a, *c* (nm)	0.80958(3)	2.2662(1)			0.80962(3)	2.2672(1)			
R_n, R_m, R_{wp}, R_{exp} (%)	3, –, 16, 2				3, 12, 16, 2				
1.5 K (HR, D1A)				μ_{xy} (μ_B)	*110 K (D1B)*				
Pr1 8f	0	0	0.1105(7)	2.6(1)	0	0	0.1105	2.6(2)	1.2(2)
Pr2 16l	0.1633(9)	0.6633(9)	0.1904(4)	2.6(1)	0.1633	0.6633	0.1904	2.5(1)	1.2(2)
Fe1 4d	0	0.5	0	0.8(2)	0	0.5	0	0.9(2)	1.2(1)
Fe2 16k	0.0685(6)	0.2091(6)	0	2.6(1)	0.0685	0.2091	0	2.1(2)	1.2(1)
Fe3 $16l_1$	0.1764(5)	0.6764(5)	0.0611(3)	2.4(1)	0.1764	0.6764	0.0611	2.3(1)	1.2(1)
Fe4 $16l_2$	0.3843(5)	0.8843(4)	0.0976(2)	2.2(1)	0.3843	0.8843	0.0976(	2.3(1)	1.2(1)
Au 4a		0	0.25		0	0	0.25		1.2(4)
a, *c* (nm)	0.80909(5)	2.2560(2)			0.8097(5)	2.2594(6)			
R_n, R_m, R_{wp}, R_{exp} (%)	4, 10, 18, 6				5, 1.4, 10, 2				

results are shown in the lower part of Fig. 6. Comparison with the data for $Pr_6Fe_{13}Ag$ shown in the top part confirms that the magnetic ordering behaviour of both compounds is essentially the same.

4. Discussion

It is well known that the 4f moments of light rare earth elements always couple ferromagnetically with the moments of 3d elements in intermetallic compounds formed between 4f and 3d elements. In fact, this type of coupling between the R and Fe moments prevails within the ferromagnetic blocks, although the Pr2 moments were shown to be more weakly coupled than the Pr1 moments.

This behaviour most probably occurs because of the location of the latter adjacent to the X layers where the sign change takes place. In the underlying crystal structure the Pr2 atoms are located between ferromagnetic Fe layers close to $z=0$ and the ferromagnetic Fe layers close to $z=1/2$. However, these two ferromagnetic Fe layers have opposite moment directions. In this position the Pr2 atoms experience frustration with regard to the coupling with the Fe moments. Because the R–R coupling is generally much smaller than the R–Fe coupling this may lead to an antiferromagnetic coupling between the two ferromagnetic Pr2 layers located on different sides of the X layers that form the boundaries of the ferromagnetic blocks mentioned above. It is interesting to note that Kajitani et al. [11] used the same type of arguments to propose an ad hoc magnetic structure for $Pr_2Fe_{13}Cu$ similar to that observed in the course of the present investigation for the corresponding Ag and Au compounds.

Several $R_6Fe_{13}X$ compounds have been investigated by Mössbauer spectroscopy. The spectra were analysed with subspectra of relative intensities corresponding to the crystallographic structure reported in Refs. [1,2] without relying on a specific magnetic structure. For the compounds $Nd_2Fe_{13}Ag$ and $Pr_6Fe_{13}Au$ the easy magnetisation direction was found [12,13] to be perpendicular to the *c*-axis, which is in agreement with the easy magnetisation direction observed for these compounds in the course of the present investigation.

Finally, we note that a comparison of LT and HT neutron patterns in the high angle region suggests lattice strains which might be related to the symmetry reduction induced by magnetoelastic coupling.

References

[1] J. Allemand, A. Letand, J.M. Moreau, J.P. Nozières, R. Perrier de la Bâthie, J. Less-Common Met. 166 (1990) 73.
[2] F. Weitzer, A. Leithe-Jasper, P. Rogl, K. Hiebl, A. Rainbacher, G. Wiesinger, J. Friedl, F.E. Wagner, J. Appl. Phys. 75 (1995) 7745.
[3] O.M. Sichevich, R.V. Lapunova, A.N. Soboley, Yu.N. Grin, Ya.P. Yarmoluk, Sov. Phys. Crystallogr. 30 (1985) 627.
[4] Q.W. Yan, P.L. Zhang, X.D. Sun, B.P. Hu, Y.Z. Wang, X.L. Rao, C.G. Liu, C. Gou, D.F. Chen, Y.F. Cheng, J. Phys.: Condensed Matter 6 (1994) 3101.
[5] F. Wang, B.-G. Shen, H. Gong, X. Sun, P. Zhang, Q. Yan, J. Magn. Magn. Mater. 177–181 (1998) 1056.
[6] B.-P. Hu, J.M.D. Coey, H. Klesnar, P. Rogl, J. Magn. Magn. Mater. 117 (1992) 225.

[7] C.H. de Groot, F.R. de Boer, K.H.J. Buschow, D. Hautot, G.J. Long, F. Grandjean, J. Alloys Comp. 233 (1996) 161.
[8] J. Rodríguez-Carvajal, Physica B 192 (1993) 55.
[9] V.A. Koptzik, Shubnikov Groups, Moscow University, 1966.
[10] W. Opechowski, R. Guccione, in: G.T. Rado, H. Suhl (Eds.), Magnetism IIA, Academic Press, London, 1965, chapt. 3, p. 105.
[11] T. Kajitani, K. Nagayama, T. Umeda, J. Magn. Magn. Mater 117 (1992) 379.
[12] G. Wiesinger, A. Rainbacher, W. Steiner, A. Leithe-Jasper, P. Rogl, F. Weitzer, Hyperfine Interactions 94 (1994) 1915.
[13] D. Hautot, G.J. Long, F. Grandjean, C.H. de Groot, K.H.J. Buschow, J. Appl. Phys. 83 (1998) 1554.